Classification: BIOLOGICAL SCIENCES, Microbiology

Controlling septum thickness by a large protein ring

Michaela Wenzel[1,§,*], Ilkay N. Celik Gulsoy[1*], Yongqiang Gao[1¤], Joost Willemse[2], Mariska G. M. van Rosmalen[3], Gijs J. L. Wuite[3], Wouter H. Roos[4], Leendert W. Hamoen[1#]

[1]Bacterial Cell Biology, Swammerdam Institute for Life Sciences, University of Amsterdam, 1098 XH Amsterdam, The Netherlands

[2]Molecular Biotechnology, Institute of Biology, Leiden University, 2333 BE, Leiden, The Netherlands

[3]Department of Physics and Astronomy and Laser Lab, Free University of Amsterdam, 1081 HV Amsterdam, The Netherlands

[4]Molecular Biophysics, Zernike Institute, University of Groningen, 9747 AG Groningen, The Netherlands

[*]These authors contributed equally to this work.

[#]Corresponding author: Leendert Hamoen, l.w.hamoen@uva.nl

[§]Current address: Division of Chemical Biology, Department of Biology and Biological Engineering, Chalmers University of Technology, 41296 Gothenburg, Sweden

[¤]Current address: Department of Microbiology and Immunobiology, Harvard Medical School, Boston MA 02115, USA

Keywords: cell division, Bacillus subtilis, FtsZ, SepF

Abstract

Gram-positive bacteria divide by forming a thick cross wall. How the thickness of this septal wall is controlled is unknown. In this type of bacteria, the key cell division protein FtsZ is anchored to the cell membrane by two proteins, FtsA and SepF. We have isolated SepF homologues from different bacterial species and found that they all polymerize into large protein rings with diameters varying from 19 to 41 nm. Importantly, these values correlated well with the thickness of their septa. To test whether ring diameter determines septal thickness, we tried to construct different SepF chimeras with the purpose to manipulate the diameter of the SepF protein ring. This was indeed possible and confirmed that the conserved core domain of SepF determines ring diameter. Importantly, when SepF chimeras with a smaller diameter were expressed in the bacterial host *Bacillus subtilis*, the thickness of its septa also became smaller. These results strongly support a model in which septal thickness is controlled by curved molecular clamps formed by SepF polymers attached to the leading edge of nascent septa. This also implies that the intrinsic shape of a protein polymer can function as a mould to shape the cell wall.

Significance Statement

Many bacteria form a thick cell wall and divide by forming a cross wall. How they control the thickness of their cell wall and cross wall is unknown. In this study we show that in these bacteria the cell division protein SepF forms very large protein rings with diameters that correspond to the diameter of their cross walls. Importantly, when we reduced the diameter of SepF rings in the bacterial host *Bacillus subtilis* the cross wall also became thinner. These results provide strong evidence that a large protein ring can function as a mould to control the thickness of the cell wall that divides these bacterial cells.

54 **Introduction**

55

56 The hallmark of Gram-positive bacteria is their thick cell wall composed of multiple
57 layers of peptidoglycan. They divide by synthesizing a crosswall in between the
58 newly formed daughter cells, and the thickness of the nascent division septum
59 approaches that of the lateral cell wall. How Gram-positive bacteria regulate the
60 thickness of their division septum is not known.

61 Bacterial cell division is accomplished by a complex multi-protein machinery
62 called the divisome. Assembly of the divisome begins with polymerization of the
63 tubulin homologue FtsZ at midcell into a ring-like configuration, the so called Z-
64 ring (1). This structure forms a scaffold for the late cell division proteins that are
65 responsible for synthesis of the dividing septal wall (2). Several cell division
66 proteins support the formation of the Z-ring, and a key step is the anchoring of
67 FtsZ polymers to the cell membrane. This is achieved by the conserved peripheral
68 membrane proteins FtsA and SepF. Both proteins directly interact with FtsZ and
69 use an amphipathic α-helix to bind the cell membrane (3, 4). FtsA can be found in
70 both Gram-positive and Gram-negative bacteria, whereas SepF is widely
71 conserved in Gram-positive and Cyanobacteria, but has no known homologue in
72 Gram-negatives (5, 6). Other Z-ring proteins are the conserved protein ZapA,
73 which interlinks FtsZ polymers (7), and the bitopic transmembrane proteins EzrA
74 (Gram-positives) and ZipA (Gram-negatives) (8, 9). Once the Z-ring is assembled,
75 the late cell division proteins arrive. These conserved transmembrane proteins
76 form a complex comprising the peptidoglycan glycosyltransferase FtsW (10), the
77 transpeptidase Pbp2B (FtsI in Gram-negatives) (11, 12), and the heterotrimeric
78 complex composed of FtsL, DivIC and DivIB (FtsL, FtsB and FtsQ in Gram-
79 negatives, respectively) (13, 14). It is assumed that the latter three proteins

80 regulate the assembly of late cell division proteins, although it is not yet clear how
81 the late proteins are recruited to the Z-ring in Gram-positive bacteria.

82 Some bacteria, such as the Gram-positive model organism *Bacillus subtilis*,
83 contain both FtsA and SepF, and this organism needs only one of them for Z-ring
84 formation. However, the absence of SepF results in highly deformed septa, which
85 is not the case when FtsA is absent (6). This indicates that SepF must have an
86 additional function related to septum formation. A curious property of purified *B.*
87 *subtilis* SepF is that it forms large ring structures with an inner diameter of 40 nm
88 (15). Based on the SepF crystal structure, these rings must encompass at least 80
89 to 100 SepF molecules (15). *In vitro*, these protein rings are able to bundle FtsZ
90 polymers into very long microtubule-like structures with SepF rings stacked
91 perpendicularly to the FtsZ polymers (16). However, such microtubular structures
92 have never been observed in bacteria, and later studies showed that the
93 membrane-binding amphipathic α-helix of SepF is likely located inside the ring,
94 which seems to rule out ring formation *in vivo* (15).

95 Interestingly, the inner diameter of SepF rings is about the same size as the
96 thickness of the septal wall (43 nm). We wondered whether this relationship is
97 relevant, and if so, whether SepF rings might actually control the thickness of the
98 septum. To examine this, we purified SepF from different Gram-positive bacteria
99 and found that all these proteins bind to lipid membranes and form large protein
100 rings, albeit with different diameters. Importantly, also in these organisms there
101 was a correlation between SepF ring diameter and septum thickness. To confirm
102 that the SepF ring diameter determines septal width, we expressed SepF chimeras
103 with smaller diameters in *B. subtilis*. Indeed, this reduced the thickness of septa.
104 These results provide strong evidence that Gram-positive bacteria regulate the
105 thickness of their septal wall by the strong curvature of SepF polymers at the

106 leading edge of nascent septa. This also implies that the intrinsic form of a protein
107 polymer can function as a mold that can shape a cell wall.

108 **Results**

109

110 **SepF rings and tubules**

111 Purified *B. subtilis* SepF forms large protein rings when observed with transmission
112 electron microscopy (TEM) using negative staining with uranyl acetate (15). To
113 confirm these findings with an independent method, we examined whether the
114 protein can form rings under more physiological conditions using atomic force
115 microscopy (AFM). It appeared that under these conditions purified *B. subtilis* SepF
116 also forms rings with diameters of 41 nm (Fig. 1). Rings were 2 to 4 nm high (Fig.
117 1C, D), which corresponds to a single or double molecule stacking, since the crystal
118 packing has shown that SepF polymers can be either 1.5 or 2.6 nm wide,
119 depending on the orientation of SepF dimers (15).

120 Previously, SepF was purified as a maltose-binding protein (MBP) fusion
121 followed by proteolytic cleavage and removal of MBP using ion-exchange
122 chromatography (15, 16). We noticed that after cleavage, SepF precipitates,
123 possibly due to the presence of calcium in the digestion buffer. After resuspension
124 in calcium-free buffer, SepF formed stacks and tubules with diameters
125 corresponding to that of SepF rings when observed by TEM (Fig. 1E). After ion-
126 exchange chromatography only rings are found (Fig. 1F). These findings, together
127 with the AFM data, show that the circular polymerization of *B. subtilis* SepF is a
128 robust feature that may also occur *in vivo*.

129

130 **SepF from other species**

131 To determine whether ring formation is a conserved feature of SepF, we purified
132 the protein from different organisms. *Bacillus cereus* is an important food-spoiling
133 bacterium (17, 18) and the causative agent of rainforest anthrax (19–21) and was

134 chosen as a close relative of *B. subtilis*. We further selected *Clostridium*
135 *perfringens*, *Mycobacterium tuberculosis*, and *Streptococcus pneumoniae,* all of
136 which are important human pathogens. *S. pneumoniae* differs from the rest since
137 it forms cocci instead of rods, and *M. tuberculosis* is one of the bacterial species
138 that lack an FtsA homologue. An amino acid sequence alignment of the different
139 SepF homologues is shown in Fig. 2A. The central domain of the protein, which
140 contains the FtsZ binding site (15), is particularly conserved. All proteins were
141 successfully purified as MBP fusions. *C. perfringens, M. tuberculosis,* and *S.*
142 *pneumoniae* SepF precipitated after proteolytic cleavage from MBP and were
143 collected by centrifugation, whereas *B. cereus* SepF remained largely soluble and
144 was isolated by ion-exchange chromatography.
145
146 **Membrane binding**
147 A key property of *B. subtilis* SepF is its capacity to bind to the cell membrane,
148 which is achieved by an N-terminal amphipathic α-helix (amino acids 1-13) (15).
149 This N-terminal amphipathic helix is reasonably conserved in the different SepF
150 variants (Fig. 2A, see Fig. S1 for helical wheel depictions), although the helices
151 differ in their hydrophobicity and hydrophobic moment (Fig. S2). To confirm that
152 the different SepF molecules are able to bind to lipid membranes, the purified
153 proteins were mixed with liposomes. This caused a strong aggregation of
154 liposomes, and deformed them into small vesicles, when observed with high-
155 resolution structured illumination microscopy (SIM). One example, *S. pneumoniae*
156 SepF, is presented in Fig. 2B, C (see Fig. S3 for all variants). Such liposome
157 deformation is a typical characteristic of membrane-interacting amphipathic α-
158 helices (22), and a *B. subtilis* SepF variant without the N-terminal α-helix does not
159 possess this property (15). These results indicate that the membrane binding

160 activity of SepF is conserved.

161

162 **Ring formation**

163 Another characteristic of *B. subtilis* SepF is its tendency to polymerize into a curved
164 structure. If this feature is important for the activity of SepF, it should not be
165 restricted to the *B. subtilis* protein. To check this, the purified SepF homologues
166 were spotted on TEM grids and negatively stained with uranyl acetate. Indeed, as
167 shown in Fig. 2D, all SepF variants formed large rings of a remarkably constant
168 size. However, the average ring diameters varied between species, from ~20 up
169 to ~40 nm (Fig. 2F).

170

171 **Correlation with septum thickness**

172 The different ring diameters provided a first proof of the hypothesis that SepF ring
173 diameter determines septum thickness. To confirm this we performed TEM of the
174 different bacterial species and measured the thickness of nascent cell division
175 septa (Fig. 2E, G). Because of its high pathogenicity we used published data for
176 *M. tuberculosis* (23). As shown in Fig. 2I, there is a clear correlation between inner
177 ring diameters and the thickness of septa in the different species. Only *B. cereus*
178 did not follow this trend, with SepF rings that are clearly smaller than the width of
179 its septa (Fig. 2F-H).

180

181 **Core domain defines ring diameter**

182 Proteolytic trimming has shown that the conserved C-terminal domain of *B. subtilis*
183 SepF, spanning amino acids 57 to 151, is sufficient for the formation of rings (15).
184 Therefore, we assumed that this core domain determines ring diameter. To test
185 this, we replaced the conserved core domain of *B. subtilis* SepF with those of the

186 SepF proteins from the other species, maintaining the first 67 and last 13 amino
187 acids of *B. subtilis* SepF. These chimeras were then expressed in *E. coli*, purified,
188 and visualized by TEM using negative staining. All SepF chimeras were able to form
189 rings, and importantly, the ring diameters of these chimeras corresponded very
190 well to the diameters of the original SepF variants (Fig. 3A-D).
191

192 **Functional chimeras**

193 If it is true that the diameter of SepF rings determines the thickness of septa, then
194 expressing a SepF variant with a smaller diameter in *B. subtilis* should result in
195 thinner septa. It is unlikely that SepF from other species function in *B. subtilis*,
196 since the N- and C-termini of SepF, which are much less conserved, are crucial for
197 its activity (15, 16). Therefore, the chimeras provided a unique opportunity to test
198 this. To determine whether these chimeras are active in *B. subtilis*, they were
199 expressed in a Δ*sepF* strain. *B. subtilis* is one of the few species that can grow
200 without SepF, although this leads to strongly deformed septa (6). Since these
201 deformed septa are lined by the cytoplasmic membrane, this phenotype can be
202 easily observed using high-resolution SIM microscopy by fluorescently labelling the
203 cell membrane (Fig. 4A). Only the *S. pneumoniae* chimera failed to rescue the
204 Δ*sepF* phenotype, while the *B. cereus, C. perfringens,* and *M. tuberculosis*
205 chimeras were all able to restore normal septum formation in the Δ*sepF*
206 background (Fig. 4A). To check that the membrane deformations observed by SIM
207 are indeed indicative of deformed cell wall septa, we confirmed these findings by
208 TEM (Fig. 4B).

209 The inner ring diameter of the *C. perfringens* SepF chimera (24 nm) is
210 considerably smaller than *B. subtilis* SepF (42 nm). When this chimera was
211 expressed in the Δ*sepF* strain, the septum thickness decreased substantially from

212 43 to 28 nm (Fig. 4C, D). A similar decrease in septum thickness was observed,
213 when the *M. tuberculosis* SepF chimera (35 nm diameter) was expressed in the
214 Δ*sepF* background (Fig. 4C-E). These results strongly suggests that the SepF ring
215 diameter control septum thickness.

216 Finally, the diameter of *B. cereus* SepF is approximately 10 nm smaller than
217 *B. subtilis* SepF (Fig. 2F), and so is the diameter of the *B. cereus* SepF chimera
218 (Fig. 3B). However, *B. cereus* has an average septum thickness comparable to that
219 of *B. subtilis* (Fig. 2G). If the core domain of SepF determines septum thickness,
220 it is likely that expression of the *B. cereus* chimera in *B. subtilis* Δ*sepF* results in
221 septa with a thickness comparable to that of wild type *B. subtilis* cells. This was
222 indeed the case (Fig. 4C-E).

223

224 **Discussion**

225

226 In this study we have shown that the membrane binding and ring forming activities
227 are conserved in SepF homologues, that the correlation between ring diameter and
228 septum thickness can be found in different Gram-positive bacteria, and that the
229 septum thickness of *B. subtilis* cells can be reduced by expressing SepF mutants
230 with a smaller diameter. Together these findings strongly suggest that the
231 diameter of curved SepF polymers define septum thickness. The positioning of
232 SepF polymers at the division site cannot be directly observed using high-
233 resolution cryo-electron microscopy due to the electron density of the bacterial
234 cytoplasm and cell wall. However, our findings provide support for a SepF clamp
235 model (Fig. 5). Since the membrane-binding amphipathic α-helix of SepF is located
236 inside the rings, it is likely that SepF polymers do not form rings, but instead form
237 arcs, wrapping the leading edge of nascent septa, on top of which FtsZ polymers
238 bind and align. Since these arcs control the freedom of movement of FtsZ
239 polymers, including the peptidoglycan synthetic apparatus that is linked to them,
240 the diameter of SepF rings will determine the thickness of the septal wall. Many
241 SepF arcs must line the leading edge of the nascent septum to maintain an even
242 thickness. This could be facilitated by the propensity of SepF rings to form stacks
243 (Fig. 1F).

244 Previous structural work has indicated that SepF rings are built of tightly
245 packed dimers. These dimers are formed by two parallel oriented monomers (15),
246 as a consequence all SepF dimers have the same orientation in a ring. However,
247 FtsZ polymers treadmill in both directions in the Z-ring (26), and it is likely that
248 they bind SepF rings in both polymer orientations. SepF binds to the C-terminal
249 domain of FtsZ (27), which is connected to the main protein domain by a long

250 flexible linker (28). This flexibility might enable FtsZ polymers with opposite
251 orientations to interact with the same SepF ring.

252 *B. cereus* SepF behaved slightly differently and showed an average inner
253 ring diameter of 30 nm, which is smaller than its average septum thickness of 43
254 nm. Possibly, *B. cereus* SepF polymers are more flexible in a cellular environment,
255 enabling a wider diameter, or there might be other factors involved in controlling
256 septum diameter in this organism in addition to the physical confinement of SepF
257 polymers. In fact, *B. subtilis* can still make septa, albeit irregular in shape, when
258 SepF is absent, suggesting that other factors provide some control of FtsZ
259 polymers. FtsA, which also forms polymers, might be such factor.

260 Gram-negative bacteria contain a cell wall that consists of a single-layer of
261 peptidoglycan. The lipoproteins LpoA and LpoB, which reach through the
262 peptidoglycan layer to contact and regulate the cell membrane-anchored
263 peptidoglycan-synthetic enzymes, are thought to regulate peptidoglycan thickness
264 in these species (24). Possibly, this is why Gram-negative bacteria do not need a
265 SepF-like protein for septum thickness control. It should be mentioned that *E. coli*
266 FtsA has been shown to form ring structures *in vitro* as well (25). However, the
267 inner diameter of these rings is ~15 nm, which is considerably smaller than the
268 width of septa.

269 Regulation of the shape of septal walls by SepF through its intrinsic
270 curvature is reminiscent of the activity of MreB, which controls the rod shape of
271 many bacteria (29). MreB forms polymers of defined curvature that orientate and
272 move transversely to the long axis of cells, along the direction of greatest
273 membrane curvature (30, 31), thereby guiding the cell wall synthetic machinery
274 in a way that enforces and maintains a rod shape (32, 33). However, unlike SepF,
275 the intrinsic curvature of MreB filaments, which has been estimated to have a

276 diameter of roughly 200 nm (30), does not correlate with the diameter of the cell,
277 which is much larger (30). Thus, the control of septum thickness by a molecular
278 clamp, such as a SepF arc, is a novel concept of how protein polymers can control
279 the shape of growing cell walls.

280 **Material and Methods**

281

282 **Strain construction**

283 All strains used in this study are listed in Table S1, plasmids in Table S2, and
284 primers in Table S3. Plasmids for purification of SepF variants were constructed by
285 PCR amplification of *sepF* from the respective organisms, followed by restriction
286 cloning into the pMalC2 plasmid (34), using the *Xba*I and *Sma*I or *Eco*RI restriction
287 sites. pMalC2-based plasmids for purification of chimera proteins and pAPNC-213-
288 kan-based plasmids (35) for integration of *sepF* variants into the *aprE* locus in the
289 *B. subtilis* genome were constructed by Gibson assembly (36). pMalC2-derived
290 purification plasmids were transformed into calcium-competent *E. coli* BL21 (DE3).
291 pAPNC-213-kan-derived integration plasmids were transformed into *B. subtilis* 168
292 using a standard starvation protocol (37). Deletions of the *sepF* and *ftsA* genes
293 were introduced by transforming the resulting *B. subtilis* strains with chromosomal
294 DNA isolated from YK204 (*sepF::spc*) (38), BFA2863 (*sepF::ery*) (6), and TB94
295 (*ftsA::cat*), respectively. TB94 was created by transformation of *B. subtilis* 168
296 with chromosomal DNA of strain MD133 *ftsA::cat aprE::kan Pspac-ftsA* (38)
297 followed by selection on chloramphenicol resistance but kanamycin sensitivity.

298

299 **Protein purification**

300 *E. coli* BL21 (DE3) strains carrying pMalC2 plasmids for purification of SepF
301 variants were grown overnight in LB containing 100 µg/ml ampicillin at 37 °C under
302 continuous shaking. Cultures were diluted 1:100 and allowed to grow until an OD_{600}
303 of 0.4 in the presence of ampicillin. Expression of maltose-binding protein (MBP)-
304 tagged SepF proteins was induced by addition of 0.5 mM IPTG. Cells were
305 harvested by centrifugation after 4 h of induction and subsequently washed in

306 phosphate-buffered saline supplemented with 1 mM phenylmethylsulfonyl fluoride
307 to prevent protein degradation. Cell pellets were flash-frozen in liquid nitrogen and
308 stored at -80 °C until further use. Cell pellets were resuspended in buffer AF (50
309 mM Tris-HCL, pH 7.4, 200 mM KCl, 5 mM EDTA, 0.5 mM DTT) supplemented with
310 one Complete mini protease inhibitor tablet (Roche) and disrupted by French Press.
311 Cell debris was removed by ultracentrifugation at 31,000 x g, and the resulting
312 supernatant was filtered through 0.2 µm filter membranes prior to loading onto a
313 Tricorn 10/20 column (GE Healthcare) packed with 2 ml amylose resin (New
314 England Biolabs) equilibrated with buffer AF. After loading, the column was washed
315 with 5 column volumes buffer AF, followed by buffer BF (50 mM Tris-HCl, pH 7.4)
316 until the baseline was stable. MBP-tagged SepF variants were eluted with buffer
317 BF containing 10 mM maltose. Appropriate fractions were pooled and digested with
318 factor Xa protease (New England Biolabs) in the presence of 2 mM $CaCl_2$ at 4 °C
319 overnight. *B. cereus* SepF was soluble while the others precipitated after cleavage
320 (*B. subtilis, S. pneumoniae, C. perfringens, M. tuberculosis,* all chimera proteins)
321 due to presence of calcium. Insoluble proteins were separated from soluble MBP
322 and factor Xa by centrifugation at 10,000 x g. Pellets containing pure SepF were
323 dissolved in buffer BF without $CaCl_2$, flash-frozen in liquid nitrogen and stored at -
324 80 °C until further use. SepF variants that were soluble after factor Xa cleavage
325 were separated from MBP and Factor Xa protease by ion exchange
326 chromatography. To this end, digested samples were loaded onto a 1 ml HiTrap Q
327 column (GE Healthcare) equilibrated with buffer BF. The column was washed with
328 buffer BF until the baseline was stable, followed by washing with 7.5% buffer CF
329 (50 mM Tris-HCl, pH 7.4, 1 M KCl) resulting in elution of MBP, and washing with
330 17.5% buffer CF resulting in elution of factor Xa. Pure SepF was eluted with 50%
331 buffer CF, flash-frozen in liquid nitrogen, and stored at -80 °C.

332

333 **Atomic force microscopy**

334 Purified *B. subtilis* SepF was diluted 1:10 in buffer BF and added onto a freshly
335 cleaved highly oriented pyrolytic graphite (HOPG) surface (Agar Scientific) and
336 allowed to settle for 20 min at room temperature prior to imaging in buffer solution
337 (39). Images were taken with an atomic force microscope from Nanotec
338 Electronica (Tres Cantos) operated in jumping mode at room temperature.
339 Olympus OMCL-RC800PSA rectangular, silicon-nitride cantilevers with a nominal
340 tip radius of 15 nm and a nominal spring constant of 0.05 N/m were used. Images
341 were processed and analyzed with WSxM software (40).

342

343 **Fluorescence light microscopy of liposomes**

344 Liposomes were prepared from *E. coli* polar lipid extract (Avanti Polar Lipids) as
345 described previously (3). Liposomes were extruded through 0.2 µm filters.
346 Samples were stained with 1 µg/ml Nile red, spotted on 1.2% agarose films,
347 covered with poly-dopamine-coated cover slips (41), and immediately imaged with
348 a Nikon Eclipse Ti equipped with a CFI Plan Apochromat DM 100x oil objective, an
349 Intensilight HG 130 W lamp, a C11440-22CU Hamamatsu ORCA camera, and NIS
350 elements software. Images were analyzed using ImageJ (National Institutes of
351 Health).

352

353 **Structured illumination (SIM) microscopy**

354 Liposomes for SIM were prepared from *E. coli* polar lipid extract (Avanti Polar
355 Lipids) as described previously (3). Liposomes were extruded through 0.8 µm
356 filters to obtain large enough vesicles. 0.25 mg/ml of the respective SepF variants
357 was mixed with 2 mg/ml liposomes in SepF binding buffer. Samples were stained

358 with 0.5 µg/ml mitotracker green, spotted on 1.2% agarose films, covered with
359 poly-dopamine-coated cover slips (41), and immediately imaged with a Nikon
360 Eclipse Ti N-SIM E microscope setup equipped with a CFI SR Apochromat TIRF
361 100x oil objective (NA1.49), a LU-N3-SIM laser unit, an Orca-Flash 4.0 sCMOS
362 camera (Hamamatsu Photonics K.K.), and NIS elements Ar software. SIM
363 microscopy of bacteria was performed by staining cells with 0.5 µg/ml mitotracker
364 green for 1 min, spotted on a thin film of 1.2% agarose (21).
365

366 **Transmission electron microscopy of proteins**

367 Protein samples were spotted on glow-discharged 200 mesh formvar/carbon-
368 coated copper grids (Agar Scientific) and incubated for 1 min at room temperature.
369 Excess liquid was removed with paper tissue and samples were negatively stained
370 by adding 100 µl 2% uranyl acetate drop by drop. Excess staining solution was
371 removed with paper tissue and samples were allowed to air dry. Samples were
372 examined with a JEOL1010 at 60 kV.
373

374 **Growth conditions for microscopy**

375 *B. cereus, S. pneumoniae*, and *C. perfringens* were grown on tryptic soy agar
376 plates containing 5 % sheep blood (BioMerieux). After three days of aerobic (*B.*
377 *cereus* and *S. pneumoniae*) or anaerobic incubation (*C. perfringens*) at 37 °C,
378 colonies were transferred to fresh plates and incubated for another 48 h prior to
379 suspension in phosphate-buffered saline and preparation for electron microscopy.
380 *B. subtilis* strains were grown in Luria-Bertani (LB) broth at 37 °C under steady
381 agitation. The medium was supplemented with 0.1 mM IPTG to induce expression
382 of SepF variants, where appropriate. It is important not to use more IPTG since
383 SepF overproduction causes membrane deformations that obscure septa (42).

384 Overnight cultures were grown with appropriate antibiotic concentrations (100
385 µg/ml spectinomycin, 10 µg/ml chloramphenicol, 5 µg/ml kanamycin, 1 µg/ml
386 erythromycin), where necessary. Cells were grown until exponential phase (OD_{600}
387 = 0.4) prior to microscopy.
388
389 **Transmission electron microscopy of bacteria**
390 Electron microscopy of bacteria was performed according to van Wezel *at al.* (43)
391 (*B. cereus*, *S. pneumoniae*, *C. perfringens)* or to a novel method that uses
392 immobilization of bacterial cells in one plane on an agarose layer prior to fixation
393 and embedding (44) (*B. subtilis*). Samples were examined with a JEOL 1010 at an
394 electron voltage of 60 kV.
395

Acknowledgements

We gratefully acknowledge Zehui Zhang and Daniel Antwi-berko for help with sample preparation, Wiep Klaas Smits for help with growing strains, Marien P. Dekker and Jan R. T. van Weering for support with TEM, and Gaurav Dugar for critically reading the manuscript. Electron microscopy was performed at the VU/VUMC EM facility, supported by the Netherlands Organization for Scientific Research (NWO, middelgroot 91111009). This work was financially supported by the Netherlands Organization for Scientific Research (NWO, STW-Vici 12128 to LWH and NWO-Vidi to WHR). MW was supported by a postdoc stipend from the Amsterdam Infection and Immunity Institute.

Conflict of Interest

The authors declare that this work was conducted in the absence of any commercial or financial relationships that could be construed as a potential conflict of interest.

Author contributions

MW planned and performed experiments and wrote the paper. INCG constructed strains and performed experiments. YG constructed strains. JW and MGM performed experiments. GJLW and WHR provided tools and planned experiments. LWH designed the study and wrote the paper.

417 **References**

418

419 1. J. Lutkenhaus, S. Pichoff, S. Du, Bacterial cytokinesis: From Z ring to
420 divisome. *Cytoskeleton* **69**, 778–790 (2012).
421 2. P. Gamba, J. W. Veening, N. J. Saunders, L. W. Hamoen, R. A. Daniel, Two-
422 step assembly dynamics of the Bacillus subtilis divisome. *J. Bacteriol.* **191**,
423 4186–4194 (2009).
424 3. H. Strahl, L. W. Hamoen, Membrane potential is important for bacterial cell
425 division. *Proc. Natl. Acad. Sci. U. S. A.* **107**, 12281–12286 (2010).
426 4. S. Pichoff, J. Lutkenhaus, Tethering the Z ring to the membrane through a
427 conserved membrane targeting sequence in FtsA. *Mol. Microbiol.* **55**, 1722–
428 1734 (2005).
429 5. J. Errington, R. A. Daniel, D.-J. Scheffers, Cytokinesis in bacteria. *Microbiol.*
430 *Mol. Biol. Rev.* **67**, 52–65, table of contents (2003).
431 6. L. W. Hamoen, J.-C. Meile, W. De Jong, P. Noirot, J. Errington, SepF, a
432 novel FtsZ-interacting protein required for a late step in cell division. *Mol.*
433 *Microbiol.* **59**, 989–999 (2006).
434 7. F. J. Gueiros-Filho, R. Losick, A widely conserved bacterial cell division
435 protein that promotes assembly of the tubulin-like protein FtsZ. *Genes*
436 *Dev.* **16**, 2544–2556 (2002).
437 8. P. A. Levin, I. G. Kurtser, A. D. Grossman, Identification and
438 characterization of a negative regulator of FtsZ ring formation in Bacillus
439 subtilis. *Proc. Natl. Acad. Sci. U. S. A.* **96**, 9642–9647 (1999).
440 9. C. A. Hale, P. A. de Boer, Direct binding of FtsZ to ZipA, an essential
441 component of the septal ring structure that mediates cell division in E. coli.
442 *Cell* **88**, 175–185 (1997).

443 10. A. Taguchi, *et al.*, FtsW is a peptidoglycan polymerase that is functional
444 only in complex with its cognate penicillin-binding protein. *Nat. Microbiol.*
445 **4**, 587–594 (2019).
446 11. R. A. Daniel, E. J. Harry, J. Errington, Role of penicillin-binding protein PBP
447 2B in assembly and functioning of the division machinery of Bacillus
448 subtilis. *Mol. Microbiol.* **35**, 299–311 (2000).
449 12. L. Wang, M. K. Khattar, W. D. Donachie, J. Lutkenhaus, FtsI and FtsW are
450 localized to the septum in Escherichia coli. *J. Bacteriol.* **180**, 2810–2816
451 (1998).
452 13. R. A. Daniel, M.-F. Noirot-Gros, P. Noirot, J. Errington, Multiple interactions
453 between the transmembrane division proteins of Bacillus subtilis and the
454 role of FtsL instability in divisome assembly. *J. Bacteriol.* **188**, 7396–7404
455 (2006).
456 14. N. Buddelmeijer, J. Beckwith, A complex of the Escherichia coli cell division
457 proteins FtsL, FtsB and FtsQ forms independently of its localization to the
458 septal region. *Mol. Microbiol.* **52**, 1315–1327 (2004).
459 15. R. Duman, *et al.*, Structural and genetic analyses reveal the protein SepF
460 as a new membrane anchor for the Z ring. *Proc. Natl. Acad. Sci. U. S. A.*
461 **110**, E4601-10 (2013).
462 16. M. E. Gündoğdu, *et al.*, Large ring polymers align FtsZ polymers for normal
463 septum formation. *EMBO J.* **30**, 617–626 (2011).
464 17. A. Kotiranta, K. Lounatmaa, M. Haapasalo, Epidemiology and pathogenesis
465 of Bacillus cereus infections. *Microbes Infect.* **2**, 189–198 (2000).
466 18. E. J. Bottone, Bacillus cereus, a volatile human pathogen. *Clin. Microbiol.*
467 *Rev.* **23**, 382–398 (2010).
468 19. K. S. Antonation, *et al.*, Bacillus cereus Biovar Anthracis Causing Anthrax in

469 Sub-Saharan Africa—Chromosomal Monophyly and Broad Geographic
470 Distribution. *PLoS Negl. Trop. Dis.* **10**, e0004923 (2016).
471 20. A. R. Hoffmaster, *et al.*, Identification of anthrax toxin genes in a Bacillus
472 cereus associated with an illness resembling inhalation anthrax. *Proc. Natl.*
473 *Acad. Sci.* **101**, 8449–8454 (2004).
474 21. C. Hoffmann, *et al.*, Persistent anthrax as a major driver of wildlife
475 mortality in a tropical rainforest. *Nature* **548**, 82 (2017).
476 22. W. A. Prinz, J. E. Hinshaw, Membrane-bending proteins. *Crit. Rev.*
477 *Biochem. Mol. Biol.* **44**, 278–291 (2009).
478 23. A. A. Velayati, P. Farnia, *Altas of Mycobacterium tuberculosis*, 1st Editio
479 (Academic Press, 2016).
480 24. A. Typas, *et al.*, Regulation of peptidoglycan synthesis by outer-membrane
481 proteins. *Cell* **143**, 1097–1109 (2010).
482 25. M. Krupka, *et al.*, Escherichia coli FtsA forms lipid-bound minirings that
483 antagonize lateral interactions between FtsZ protofilaments. *Nat. Commun.*
484 **8**, 15957 (2017).
485 26. A. W. Bisson-Filho, *et al.*, Treadmilling by FtsZ filaments drives
486 peptidoglycan synthesis and bacterial cell division. *Science* **355**, 739–743
487 (2017).
488 27. E. Krol, *et al.*, Bacillus subtilis SepF binds to the C-terminus of FtsZ. *PLoS*
489 *One* **7**, e43293 (2012).
490 28. P. J. Buske, A. Mittal, R. V Pappu, P. A. Levin, An intrinsically disordered
491 linker plays a critical role in bacterial cell division. *Semin. Cell Dev. Biol.*
492 **37**, 3–10 (2015).
493 29. L. J. Jones, R. Carballido-Lopez, J. Errington, Control of cell shape in
494 bacteria: helical, actin-like filaments in Bacillus subtilis. *Cell* **104**, 913–922

495 (2001).
496 30. S. Hussain, *et al.*, MreB filaments align along greatest principal membrane
497 curvature to orient cell wall synthesis. *Elife* **7**, e32471 (2018).
498 31. T. S. Ursell, *et al.*, Rod-like bacterial shape is maintained by feedback
499 between cell curvature and cytoskeletal localization. *Proc. Natl. Acad. Sci.*
500 *U. S. A.* **111**, E1025-34 (2014).
501 32. J. Dominguez-Escobar, *et al.*, Processive movement of MreB-associated cell
502 wall biosynthetic complexes in bacteria. *Science* **333**, 225–228 (2011).
503 33. E. C. Garner, *et al.*, Coupled, circumferential motions of the cell wall
504 synthesis machinery and MreB filaments in B. subtilis. *Science* **333**, 222–
505 225 (2011).
506 34. P. Riggs, "Expression and Purification of Maltose-Binding Protein Fusions" in
507 *Current Protocols in Molecular Biology*, (John Wiley & Sons, Inc., 2001)
508 https:/doi.org/10.1002/0471142727.mb1606s28.
509 35. M. Yoshimura, T. Oshima, N. Ogasawara, Involvement of the YneS/YgiH
510 and PlsX proteins in phospholipid biosynthesis in both Bacillus subtilis and
511 Escherichia coli. *BMC Microbiol.* **7**, 69 (2007).
512 36. D. G. Gibson, *et al.*, Enzymatic assembly of DNA molecules up to several
513 hundred kilobases. *Nat Meth* **6**, 343–345 (2009).
514 37. P. M. Hauser, D. Karamata, A rapid and simple method for Bacillus subtilis
515 transformation on solid media. *Microbiology* **140**, 1613–1617 (1994).
516 38. S. Ishikawa, Y. Kawai, K. Hiramatsu, M. Kuwano, N. Ogasawara, A new
517 FtsZ-interacting protein, YlmF, complements the activity of FtsA during
518 progression of cell division in Bacillus subtilis. *Mol. Microbiol.* **60**, 1364–
519 1380 (2006).
520 39. K. Heinze, *et al.*, Protein Nanocontainers from Nonviral Origin: Testing the

521 Mechanics of Artificial and Natural Protein Cages by AFM. *J. Phys. Chem. B*
522 **120**, 5945–5952 (2016).
523 40. I. Horcas, *et al.*, WSXM: A software for scanning probe microscopy and a
524 tool for nanotechnology. *Rev. Sci. Instrum.* **78**, 13705 (2007).
525 41. J. D. te Winkel, D. A. Gray, K. H. Seistrup, L. W. Hamoen, H. Strahl,
526 Analysis of antimicrobial-triggered membrane depolarisation using voltage
527 sensitive dyes. *Front. Cell Dev. Biol.* **4**, 29 (2016).
528 42. Y. Gao, M. Wenzel, M. J. Jonker, L. W. Hamoen, Free SepF interferes with
529 recruitment of late cell division proteins. *Sci. Rep.* **7**, 16928 (2017).
530 43. G. P. van Wezel, *et al.*, ssgA is essential for sporulation of Streptomyces
531 coelicolor A3(2) and affects hyphal development by stimulating septum
532 formation. *J. Bacteriol.* **182**, 5653–5662 (2000).
533 44. D. Saeloh, *et al.*, The novel antibiotic rhodomyrtone traps membrane
534 proteins in vesicles with increased fluidity. *PLoS Pathog.* **14**, e1006876
535 (2018).
536

537 **Figure legends**

538

539 **Fig. 1** SepF forms rings and tubules. **(A)** Plane AFM images of three different SepF
540 rings imaged in buffer solution. **(B)** 3D projections of the same images. **(C)** Height
541 measurements of the individual SepF rings shown in A and B. **(D)** Height
542 measurements of SepF rings derived from AFM data. **(E)** TEM image of SepF stack
543 and tubules after cleavage from MBP. **(F)** TEM image of SepF rings after ion-
544 exchange chromatography. Scale bars 100 nm.

545

546 **Fig. 2** Membrane binding, ring formation and septum thickness. **(A)** Sequence
547 alignment (Clustal Omega) of SepF homologues used in this study. Dark and light
548 grey marks identical and similar amino acids, respectively. Arrows mark the
549 beginning and end of the highly conserved core domain. **(B)** Fluorescence light
550 microscopy image showing the aggregation of small liposomes (~200 nm) by
551 purified *S. pneumoniae* SepF. Liposomes were stained with Nile red. **(C)** SIM image
552 showing deformation of large liposomes (800 nm) by purified *S. pneumoniae* SepF.
553 Liposomes were stained with mitotracker green. 0.25 µg/ml SepF was mixed with
554 2 mg/ml liposomes. Scale bars 1 µm. See Fig. S3 for the results with other SepF
555 variants. **(D)** TEM pictures of purified SepF from the different species. Scale bar
556 50 nm. **(E)** Quantification of the inner SepF ring diameter. Ring diameter was
557 consistently measured as the inner diameter of the SepF ring at its widest point.
558 Black bars show mean with standard error of the mean. A minimum of 45 rings
559 was measured. **(F)** TEM images of nascent cell division septa of the respective
560 species. **(G)** Quantification of the thickness of the nascent septa of the respective
561 organisms. Black bars show mean with standard error of the mean. A minimum of
562 50 septa was measured. **(H)** Comparison of inner ring diameters with nascent

563 septum thickness. Average +/- standard deviations is indicated. *Data for *M.*
564 *tuberculosis* were taken from the literature (23). **(I)** Correlation between inner
565 SepF ring diameter and septum thickness (R^2=0.74).
566
567 **Fig. 3** The conserved core domain of SepF determines ring diameter. **(A)** TEM
568 pictures of purified SepF chimera proteins. **(B)** Quantification of ring diameter.
569 Black bars represent mean with standard error of the mean. A minimum of 50
570 rings was measured. **(C)** Comparison of the inner ring diameters of the original
571 and chimera proteins. Average +/- standard deviation is given. **(D)** Correlation
572 between original and chimera ring diameter (R^2=0.71).
573
574 **Fig. 4** SepF ring diameter determines septum thickness. **(A)** SIM images of *B.*
575 *subtilis* Δ*sepF* cells expressing different SepF chimeras. The chimeras were
576 expressed from the IPTG-inducible *Pspac* promotor. Cells were grown in the
577 presence of 100 µM IPTG until mid-log phase prior to membrane staining and
578 microscopy. Lack of SepF results in severely deformed septa, which shows as
579 highly fluorescent membrane patches due to membrane invaginations and double
580 membranes. Scale bar 2 µm. **(B)** Representative TEM images of septa of Δ*sepF*
581 strains expressing the different SepF chimeras. Scale bar 1 µm. **(C)** Quantification
582 of the septum thickness of the different strains. Black bars represent mean with
583 standard error of the mean. p values for *C. perfringens* and *M. tuberculosis*
584 chimeras compared to *B. subtilis* are <0.0001. **(D)** Comparison and **(E)** correlation
585 of the inner ring diameter of SepF chimeras and nascent septum thickness of *B.*
586 *subtilis* Δ*sepF* expressing the chimeras (R^2=0.57).
587
588 **Fig. 5** Clamp model illustrating how SepF polymers can control septal thickness.

589 SepF forms large rings with an average inner ring diameter (d) that corresponds
590 to the thickness of septa (t). Crossections of a nascent septum (grey) is depicted.
591 FtsZ polymers (Z) bind to the outside of SepF rings, in a perpendicular fasion. The
592 transmembrane peptidoglycan synthesis machinery (P) is associated with FtsZ
593 polymers. Of note, it is not yet know how these transmembrane proteins are linked
594 to FtsZ polymers in Gram-positive bacteria, and this association might be indirect.

Fig. 1.

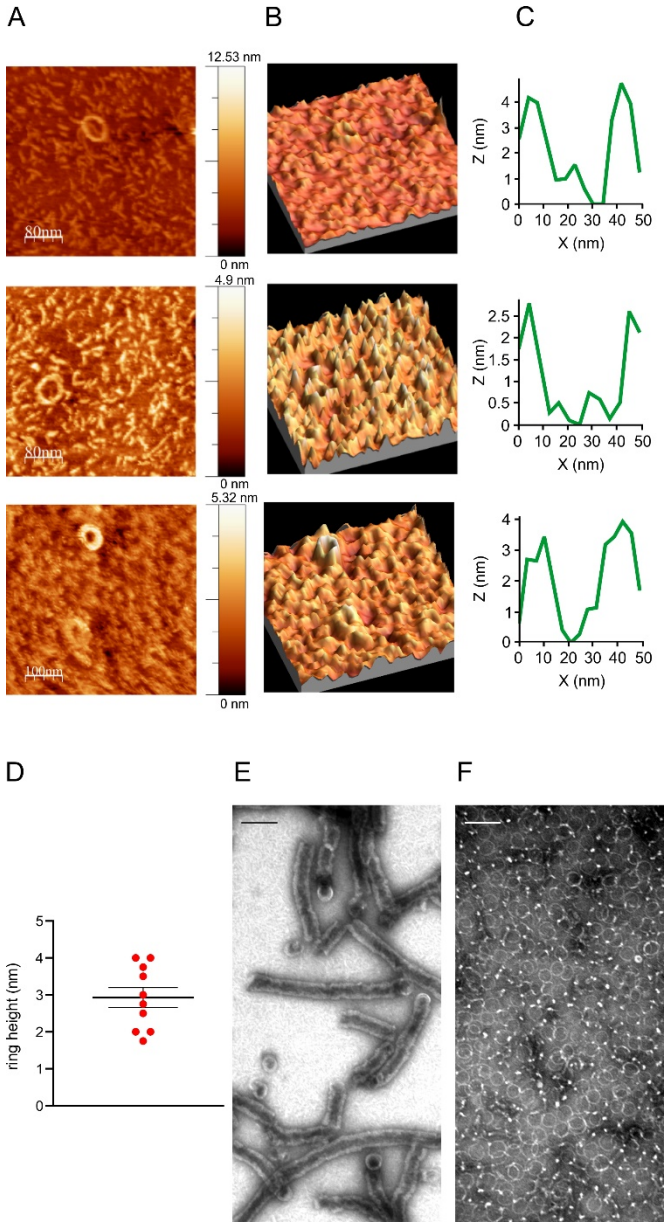

Fig. 1 SepF forms rings and tubules. **(A)** Plane AFM images of three different SepF rings imaged in buffer solution. **(B)** 3D projections of the same images. **(C)** Height measurements of the individual SepF rings shown in A and B. **(D)** Height measurements of SepF rings derived from AFM data. **(E)** TEM image of SepF stack and tubules after cleavage from MBP. **(F)** TEM image of SepF rings after ion-exchange chromatography. Scale bars 100 nm.

Fig. 2.

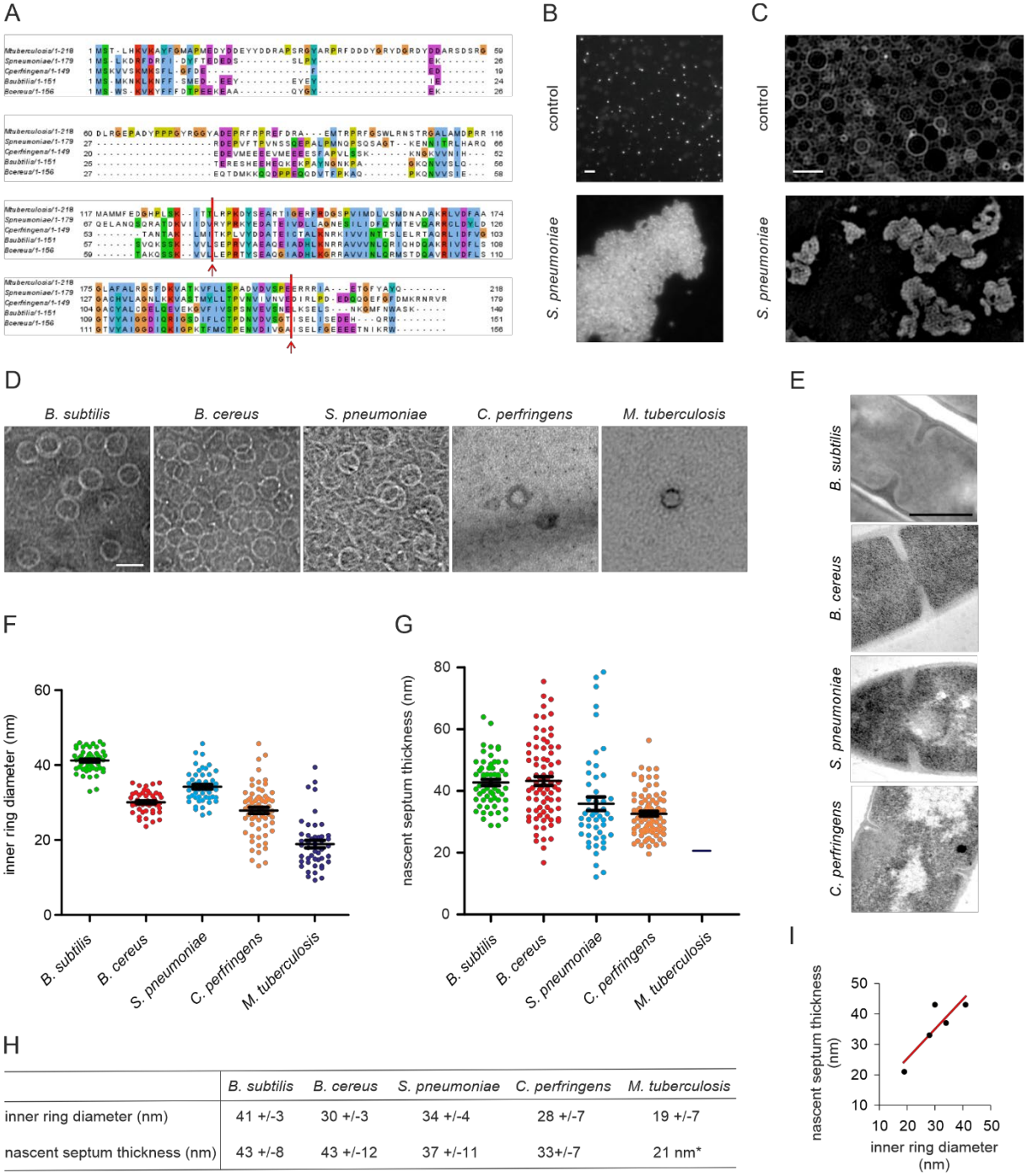

H

	B. subtilis	*B. cereus*	*S. pneumoniae*	*C. perfringens*	*M. tuberculosis*
inner ring diameter (nm)	41 +/-3	30 +/-3	34 +/-4	28 +/-7	19 +/-7
nascent septum thickness (nm)	43 +/-8	43 +/-12	37 +/-11	33+/-7	21 nm*

Fig. 2 Membrane binding, ring formation and septum thickness. **(A)** Sequence alignment (Clustal Omega) of SepF homologues used in this study. Dark and light grey marks identical and similar amino acids, respectively. Arrows mark the beginning and end of the highly conserved core domain. **(B)** Fluorescence light microscopy image showing the aggregation of small liposomes (~200 nm) by purified *S. pneumoniae* SepF. Liposomes were stained with Nile red. **(C)** SIM image showing deformation of large liposomes (800 nm) by purified *S. pneumoniae* SepF. Liposomes were stained with mitotracker green. 0.25 µg/ml SepF was mixed with

691 2 mg/ml liposomes. Scale bars 1 µm. See Fig. S3 for the results with other SepF
692 variants. **(D)** TEM pictures of purified SepF from the different species. Scale bar
693 50 nm. **(E)** Quantification of the inner SepF ring diameter. Ring diameter was
694 consistently measured as the inner diameter of the SepF ring at its widest point.
695 Black bars show mean with standard error of the mean. A minimum of 45 rings
696 was measured. **(F)** TEM images of nascent cell division septa of the respective
697 species. **(G)** Quantification of the thickness of the nascent septa of the respective
698 organisms. Black bars show mean with standard error of the mean. A minimum of
699 50 septa was measured. **(H)** Comparison of inner ring diameters with nascent
700 septum thickness. Average +/- standard deviations is indicated. *Data for *M.*
701 *tuberculosis* were taken from the literature (23). **(I)** Correlation between inner
702 SepF ring diameter and septum thickness (R^2=0.74).

Fig. 3.

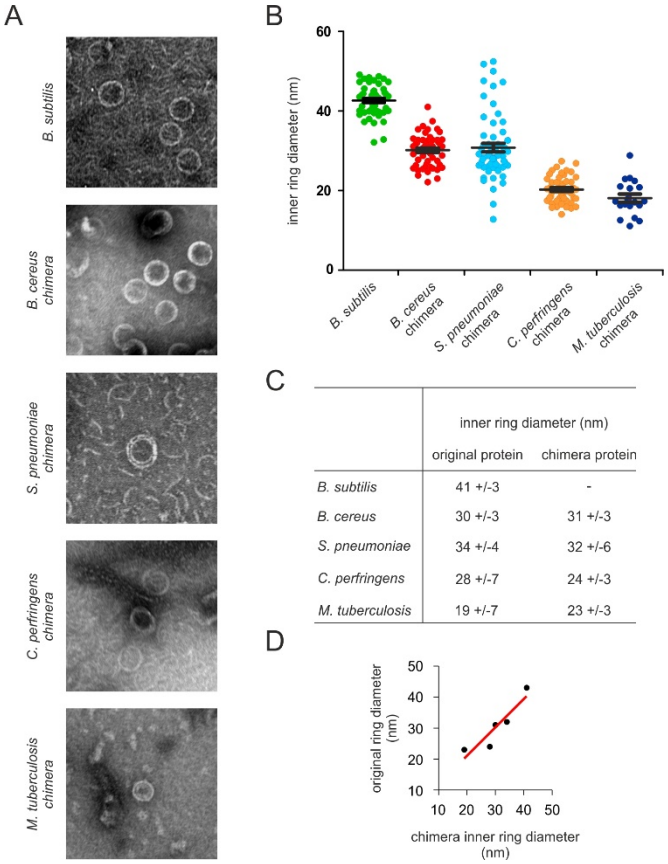

	inner ring diameter (nm)	
	original protein	chimera protein
B. subtilis	41 +/-3	-
B. cereus	30 +/-3	31 +/-3
S. pneumoniae	34 +/-4	32 +/-6
C. perfringens	28 +/-7	24 +/-3
M. tuberculosis	19 +/-7	23 +/-3

Fig. 3 The conserved core domain of SepF determines ring diameter. **(A)** TEM pictures of purified SepF chimera proteins. **(B)** Quantification of ring diameter. Black bars represent mean with standard error of the mean. A minimum of 50 rings was measured. **(C)** Comparison of the inner ring diameters of the original and chimera proteins. Average +/- standard deviation is given. **(D)** Correlation between original and chimera ring diameter (R^2=0.71).

Fig. 4.

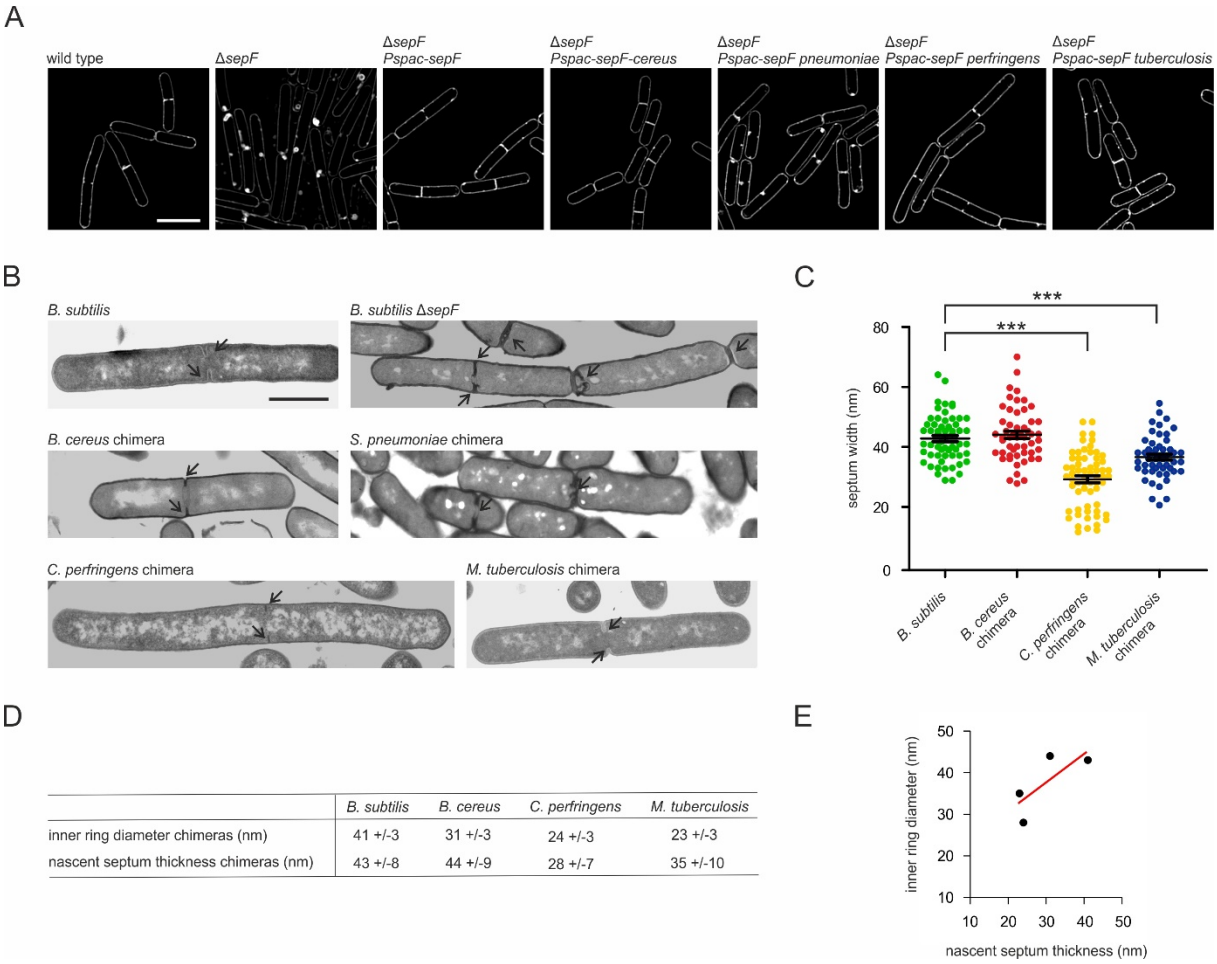

D

	B. subtilis	B. cereus	C. perfringens	M. tuberculosis
inner ring diameter chimeras (nm)	41 +/-3	31 +/-3	24 +/-3	23 +/-3
nascent septum thickness chimeras (nm)	43 +/-8	44 +/-9	28 +/-7	35 +/-10

Fig. 4 SepF ring diameter determines septum thickness. **(A)** SIM images of *B. subtilis* Δ*sepF* cells expressing different SepF chimeras. The chimeras were expressed from the IPTG-inducible *Pspac* promotor. Cells were grown in the presence of 100 µM IPTG until mid-log phase prior to membrane staining and microscopy. Lack of SepF results in severely deformed septa, which shows as highly fluorescent membrane patches due to membrane invaginations and double membranes. Scale bar 2 µm. **(B)** Representative TEM images of septa of Δ*sepF* strains expressing the different SepF chimeras. Scale bar 1 µm. **(C)** Quantification of the septum thickness of the different strains. Black bars represent mean with standard error of the mean. p values for *C. perfringens* and *M. tuberculosis* chimeras compared to *B. subtilis* are <0.0001. **(D)** Comparison and **(E)** correlation of the inner ring diameter of SepF chimeras and nascent septum thickness of *B. subtilis* Δ*sepF* expressing the chimeras (R^2=0.57).

Fig. 5.

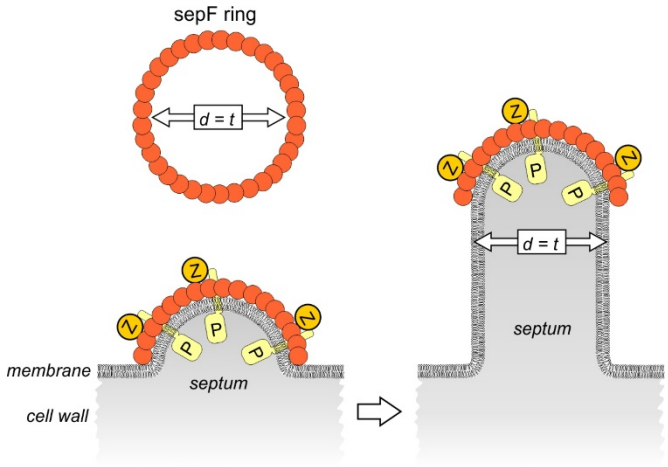

Fig. 5 Clamp model illustrating how SepF polymers can control septal thickness. SepF forms large rings with an average inner ring diameter (d) that corresponds to the thickness of septa (t). Crossections of a nascent septum (grey) is depicted. FtsZ polymers (Z) bind to the outside of SepF rings, in a perpendicular fasion. The transmembrane peptidoglycan synthesis machinery (P) is associated with FtsZ polymers. Of note, it is not yet know how these transmembrane proteins are linked to FtsZ polymers in Gram-positive bacteria, and this association might be indirect.

Supplementary Information

Controlling septum thickness by a large protein ring

Michaela Wenzel, Ilkay N. Celik Gulsoy, Yongqiang Gao, Joost Willemse, Mariska G. M. van Rosmalen, Gijs J. L. Wuite, Wouter H. Roos, Leendert W. Hamoen

- **Table S1** Strains used in this study
- **Table S2** Plasmids used in this study
- **Table S3** Primers used in this study
- **Fig. S1** Comparison of the amphipathic helices of SepF variants
- **Fig. S2** Hydrophobic moment plot of the putative N-terminal α-helices of SepF variants
- **Fig. S3** Liposome aggregation and deformation by SepF variants
- **References**

Table S1 Strains used in this study.

strains	***genotype***	***reference***
B. subtilis 168	*trpC2*	(1)
B. subtilis TB92	*trpC2 sepF::spc* (YK204 in 168CA)	(2)
B. subtilis TB94	*trpC2 ftsA::cat* (MD133 in 168CA)	(2)
B. subtilis LH28	*trpC2 ezrA::cat*	(3)
B. subtilis BFA2863	*trpC2 sepF::ery*	(4)
B. subtilis GYQ457	*trpC2 aprE::kan Pspac-sepF(subtilis-cereus)*	this study
B. subtilis GYQ475	*trpC2 aprE::kan Pspac-sepF(subtilis-pneumoniae)*	this study
B. subtilis GYQ544	*trpC2 aprE::kan Pspac-sepF(subtilis-perfringens)*	this study
B. subtilis GYQ474	*trpC2 aprE::kan Pspac-sepF(subtilis-tuberculosis)*	this study
B. subtilis MW18	*trpC2 aprE::kan Pspac-sepF(WT) sepF::spc*	this study
B. subtilis GYQ458	*trpC2 aprE::kan Pspac-sepF(subtilis-cereus)*	this study
B. subtilis MW89	*trpC2 aprE::kan Pspac-sepF(subtilis-pneumoniae)*	this study
B. subtilis MW92	*trpC2 aprE::kan Pspac-sepF(subtilis-perfringens)*	this study
B. subtilis MW86	*trpC2 aprE::kan Pspac-sepF(subtilis-tuberculosis)*	this study
E. coli BL21(DE03) pNC1	*pMalC2-sepF(coelicolor3)*	this study
E. coli BL21(DE03) pNC2	*pMalC2-sepF(cereus)*	this study
E. coli BL21(DE03) pNC4	*pMalC2-sepF(tuberculosis)*	this study
E. coli BL21(DE03) pNC5	*pMalC2sepF(coelicolor2)*	this study
E. coli BL21(DE03) pNC6	*pMalC2-sepF(coelicolor1)*	this study
E. coli BL21(DE03) pNC7	*pMalC2-sepF(perfringens)*	this study
E. coli BL21(DE03) pNC9	*pMalC2-sepF(pneumoniae)*	this study
E. coli BL21(DE03) pNC12	*pMalC2-sepF(subtilis)*	(5)
E. coli BL21(DE03) pYQ62	*pMalC2-sepF(subtilis-cereus)*	this study
E. coli BL21(DE03) pYQ94	*pMalC2-sepF(subtilis-tuberculosis)*	this study
E. coli BL21(DE03) pYQ95	*pMalC2-sepF(subtilis-perfringens)*	this study
E. coli BL21(DE03) pYQ96	*pMalC2-sepF(subtilis-pneumoniae)*	this study
B. cereus ATCC14579		(6)
S. pneumoniae ATCC6305		(7, 8)
C. perfringens ATCC13124		(9)

Table S2 Plasmids used in this study.

plasmid	genotype	reference
pMW8	*pAPNC-213-kan-Pspac-sepF(WT)*	this study
pYQ90	*pAPNC-213-kan-Pspac-sepF(subtilis-cereus)*	this study
pYQ97	*pAPNC-213-kan-Pspac-sepF(subtilis-tuberculosis)*	this study
pYQ98	*pAPNC-213-kan-Pspac-sepF(subtilis-perfringens)*	this study
pYQ99	*pAPNC-213-kan-Pspac-sepF(subtilis-pneumoniae)*	this study
pNC1	*pMalC2-sepF(coelicolor3)*	this study
pNC2	*pMalC2-sepF(cereus)*	this study
pNC4	*pMalC2-sepF(tuberculosis)*	this study
pNC5	*pMalC2sepF(coelicolor2)*	this study
pNC6	*pMalC2-sepF(coelicolor1)*	this study
pNC7	*pMalC2-sepF(perfringens)*	this study
pNC9	*pMalC2-sepF(pneumoniae)*	this study
pNC12	*pMalC2-sepF(subtilis)*	(5)
pYQ62	*pMalC2-sepF(subtilis-cereus)*	this study
pYQ94	*pMalC2-sepF(subtilis-tuberculosis)*	this study
pYQ95	*pMalC2-sepF(subtilis-perfringens)*	this study
pYQ96	*pMalC2-sepF(subtilis-pneumoniae)*	this study

Table S3 Primers used in this study.

primer	***description***	***sequence***	***used for***
MW135	pAPNC-213-kan-GA-for	GGCGTTAGCCCAAGCGC	pMW8
MW139	pAPNC-213-kan-GA-rev	ACACCCCCTGTTTCATTTCCCTAGCAGGTCAATTGTGAGCGC	pMW8
MW140	*sepF*-WT-GA-for	GGAAATGAAACAGGGGGTGTACAGCAATGAGTATGAAAAATAAACTGAAAAACTTTTTCTCAATGGAAGATGAAG	pMW8
MW141	*sepF*-WT-GA-rev	GCGCTTGGGCTAACGCCTTACCACCTCTGATGTTCGTCTTCAGATATG	pMW8
eg122	*sepF-cereus*-for	GACGAATTCATGAGTTGGTCAAAAG	pNC2
eg123	*sepF-cereus*-rev	GACTCTAGATTACCACCTCTTTAT	pNC2
inc15	*sepF-pneumoniae*-for	GTAGGAGCCCGGGATGTCTTTAAAAGATAG	pNC9
inc16	*sepF-pneumoniae*-rev	GCTAGACTCTAGATTATCGTACTCTATTTC	pNC9
inc9	*sepF-perfringens*-for	GATTAGCCCGGGATGTGTATGTCAAAAG	pNC7
inc10	*sepF-perfringens*-rev	GACTATCTAGATTATTTTGAAGCCCAGTTG	pNC7
inc7	*sepF-tuberculosis*-for	GGTTACGGAATTCGTGAATAGTCACTGTAG	pNC4
inc8	*sepF-tuberculosis*-rev	GGCGACCGTCTAGACTATTGGTAGGCGTAG	pNC4
inc17	*sepF-coelicolor* 1-for	GTGAGAGGAGGAATTCATGGGATCGGTAC	pNC6
inc18	*sepF-coelicolor* 1-rev	TGTGCGGCTCTAGATCAGCTCTGGTTGAAG	pNC6
inc19	*sepF-coelicolor* 2-for	GAGGACTCCCGGGATGGCCGGCGCGATG	pNC5
inc20	*sepF-coelicolor* 2-rev	ACCGGTAGTCTAGATCAGCTCTGGTTGAAG	pNC5
eg139	*sepF-coelicolor* 3-for	GACGAATTCGTGAAATCGGGGGAGC	pNC1
eg140	*sepF-coelicolor* 3-rev	GACTCTAGATCACACTCCCGGCAC	pNC1
YQ276	*sepF-cereus*-for	AATCCTCTAAAGTGGTGTTGTTAGAACCACGCACATATTCGGA	pYQ62, 90
YQ277	*sepF-cereus*-rev	CGCACCAACAATATCTACATTTTC	pYQ62, 90
YQ278	pMalC2-for	ATGTAGATATTGTTGGTGCGATTTCTGAGCTCATATCTGAAGAC	pYQ62, 90
YQ279	pMalC2-rev	CAACACCACTTTAGAGGATTTCTG	pYQ62, 90
YQ349	pMalC2-rev	TTTCTGAACACTTTGCAAGCTCAC	pYQ94-99
YQ350	*sepF-tuberculosis*-for	GAGCTCATATCTGAAGACGAACATC	pYQ94, 97
YQ351	pMalC2-for	GCTTGCAAAGTGTTCAGAAACTCTCGAAGATCACCACGCT	pYQ94-99
YQ352	*sepF-tuberculosis*-rev	TCGTCTTCAGATATGAGCTCGCGCTCCTCGGGGGACACATC	pYQ94, 97
YQ353	*sepF-perfringens*-	GCTTGCAAAGTGTTCAGAAAACAGCTAAATTA	pYQ95, 98

	for	ATGATAACTAAACCA	
YQ354	*sepF-perfringens*-rev	TCGTCTTCAGATATGAGCTCCTTTAATTCATTGCTTACTTCAAC	pYQ95, 98
YQ355	*sepF-pneumoniae*-for	GCTTGCAAAGTGTTCAGAAAAAGGTCATTATAGATGTTCGTTATC	pYQ96, 99
YQ356	*sepF-pneumoniae*-rev	TCGTCTTCAGATATGAGCTCGATATCTTCAACATTTACAATAACATTC	pYQ96, 99

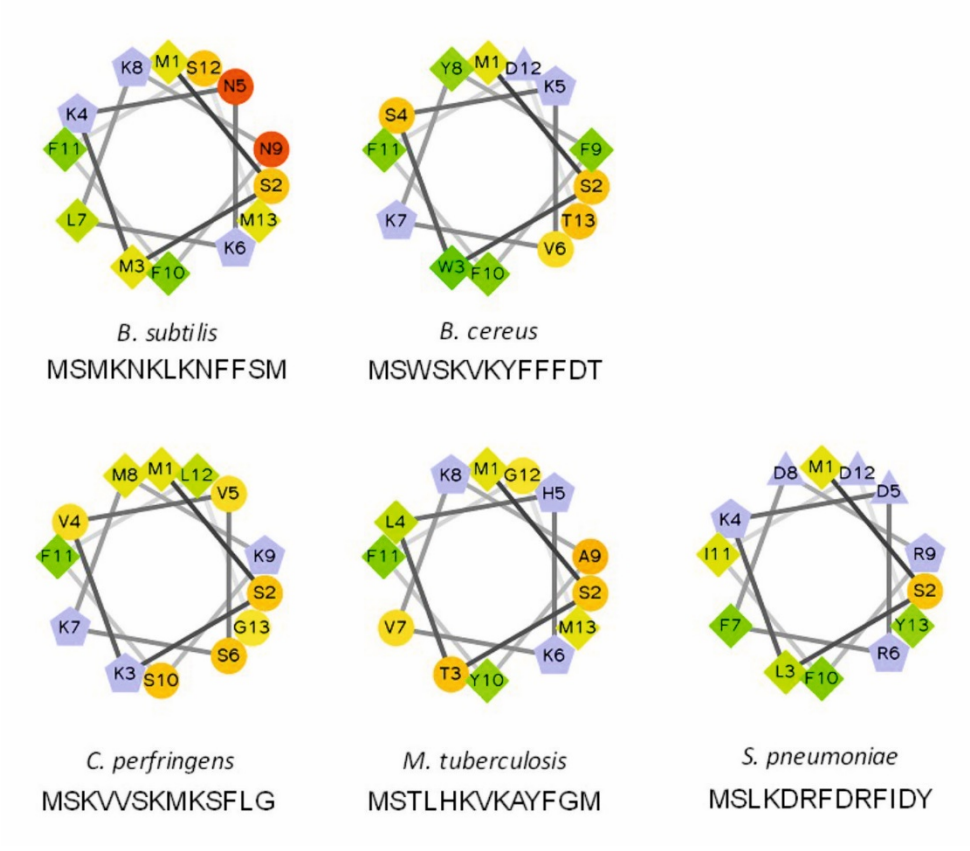

Fig. S1 Comparison of the amphipathic helices of SepF variants. Helical wheel projections (RZ lab) show the first 13 amino acids of the different proteins. Hydrophilic residues are represented as circles, hydrophobic residues as diamonds, negatively charged as triangles, and positively charged as pentagons. Hydrophobicity is color coded with green indicating the highest and yellow the lowest (zero) hydrophobicity. Hydrophilic residues are depicted in red with the amount of red decreasing to orange proportionally to the hydrophilicity. Potentially charged residues are depicted in light blue.

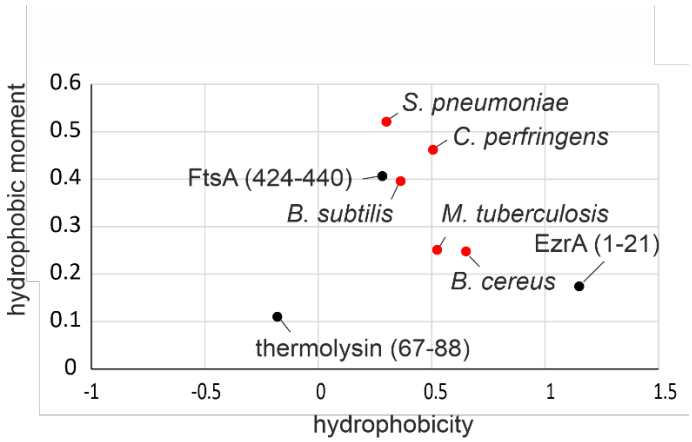

Fig. S2 Hydrophobic moment plot of the putative N-terminal α-helices of SepF variants. High H values indicate strong hydrophobicity. The hydrophobic moment (μH) is a measure for the amphipathicity of an α-helix (high values indicating strong amphipathicity). The plot of H and μH indicates the probability of an α-helix to reside in the globular or surface-exposed domains of a protein and can be used to predict transmembrane or amphipathic membrane-binding helices. Black dots indicate known globular (*Bacillus thermoproteolyticus* thermolysin, aa 67-88), transmembrane (*B. subtilis* EzrA, aa 1-21) and amphipathic (*B. subtilis* FtsA, aa 424-440) helices for comparison. N-terminal α-helices of SepF homologues are depicted in red.

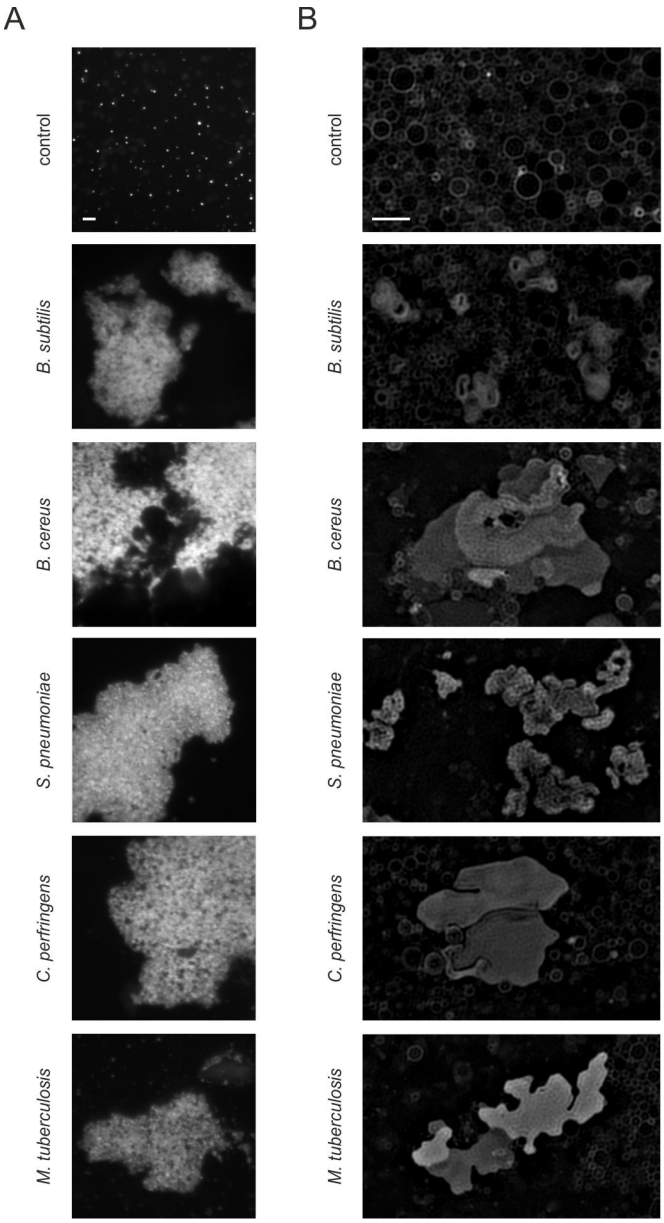

Fig. S3 Liposome aggregation and deformation by SepF variants. **(A)** Fluorescence light microscopy images of small liposomes (200 nm) stained with Nile red. **(B)** SIM images of large liposomes (800 nm) stained with mitotracker green. 0.25 µg/ml of the different SepF proteins (species names indicated) were mixed with 2 mg/ml liposomes prepared from *E. coli* polar lipid extract. Scale bars 1 µm.

References

1. Anagnostopoulos C, Spizizen J (1960) Requirements for transformation in Bacillus subtilis. *J Bacteriol* 81(5):741–746.
2. Ishikawa S, Kawai Y, Hiramatsu K, Kuwano M, Ogasawara N (2006) A new FtsZ-interacting protein, YlmF, complements the activity of FtsA during progression of cell division in Bacillus subtilis. *Mol Microbiol* 60(6):1364–1380.
3. Gamba P, Rietkotter E, Daniel RA, Hamoen LW (2015) Tetracycline hypersensitivity of an ezrA mutant links GalE and TseB (YpmB) to cell division. *Front Microbiol* 6:346.
4. Hamoen LW, Meile J-C, De Jong W, Noirot P, Errington J (2006) SepF, a novel FtsZ-interacting protein required for a late step in cell division. *Mol Microbiol* 59(3):989–999.
5. Duman R, et al. (2013) Structural and genetic analyses reveal the protein SepF as a new membrane anchor for the Z ring. *Proc Natl Acad Sci U S A* 110(48):E4601-10.
6. Frankland GC, Frankland PF (1887) XI. Studies on some new micro-organisms obtained from air. *Philos Trans R Soc London* 178:257–287.
7. Public Health Weekly Reports for APRIL 14, 1944 (1944) *Public Heal reports (Washington, DC 1896)* 59(15):485–512.
8. Public Health Weekly Reports for APRIL 7, 1944 (1944) *Public Heal reports (Washington, DC 1896)* 59(14):449–484.
9. Eastoe JE, Long JE (1959) The effect of nisin on the growth of cels and spores of Clostridium welchii in gelatine. *J Appl Bacteriol* 22(1):1–7.